

## Scattered Light in the STIS Echelle Modes

W. Landsman

*Hughes STX, NASA/GSFC, Greenbelt, MD 20771*

C. Bowers

*NASA/GSFC, Greenbelt, Maryland 20771*

### 1. Introduction

The STIS echelle spectra obtained during the Early Release Observations (Heap et al. 1997, Walborn et al. 1997, Jenkins et al. 1997) have non-zero residuals in the cores of saturated interstellar lines, indicating the need for a scattered light correction. A rough measure of the magnitude of the needed correction is given in Figures 1 and 2, which show the ratio of the interorder to the in-order flux in different echelle modes in both pre-launch calibration images of a continuum lamp source (Figure 1), and in post-launch images of stellar continuum sources (Figure 2). The interorder and in-order fluxes are computed by averaging the central 200 pixels in the dispersion direction. The amount of scattered light in the interorder region rises toward shorter wavelengths for two reasons: (1) the order separation decreases toward shorter wavelengths, and (2) the amount of echelle scattering is expected to have an inverse dependence on wavelength (e.g., Cardelli, Ebbets & Savage 1990). At the shortest wavelengths the fraction of light scattered into the interorder region can be 10% for the NUV-MAMA and 15% for the FUV-MAMA.

### 2. Sources of Scattered Light

The strong narrow emission lines of deep platinum line lamp WAVECAL images can be used to isolate the scattering sources in the echelle modes. Figure 3 shows a very deep NUV-MAMA line lamp image taken during the pre-launch calibration, while Figure 4 shows the deepest line lamp image thus far obtained during flight. Both images were obtained with the 0".1 by 0".09 slit. These images do not show extended wings perpendicular to the orders, indicating that the contribution of cross-disperser grating scattered light is negligible. Instead, the two main sources of scattered light are the following:

1. A detector halo surrounds the strong emission lines. This halo is never larger than about 16 pixels in radius. This value should be compared with the interorder spacing, which is about 15 pixels at the shortest wavelengths of both MAMA detectors, and about 40–50 pixels at the longest wavelengths. The size of the detector halo is larger in the NUV-MAMA and has a radius increasing with increasing wavelength.
2. Scattering from the echelle gratings causes a continuum which connects the appearance of an emission line in different orders. Note that this source of scattered light is very “non-local”.

Two minor sources of scattered light can also be seen in Figures 3 and 4. First, reflections in the optical path cause a secondary image of the emission lines, as seen at about “five o’clock” off the edge of the haloes of the strong lines. Second, the emission lines near the bottom edge of the NUV-MAMA detector show vertical spikes, whose origin is presently uncertain.

Figure 1. Ratio of interorder to in-order flux for ground calibration data. Each plot includes data from at least two images (marked with different symbols).

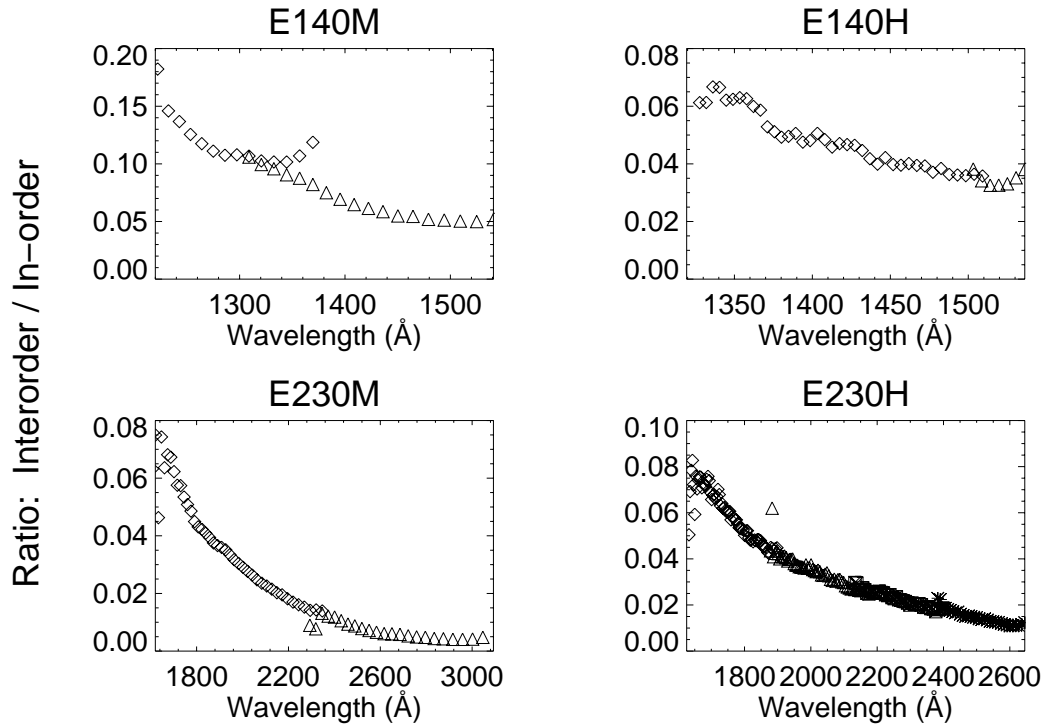


Figure 2. Ratio of interorder to in-order flux for flight data.

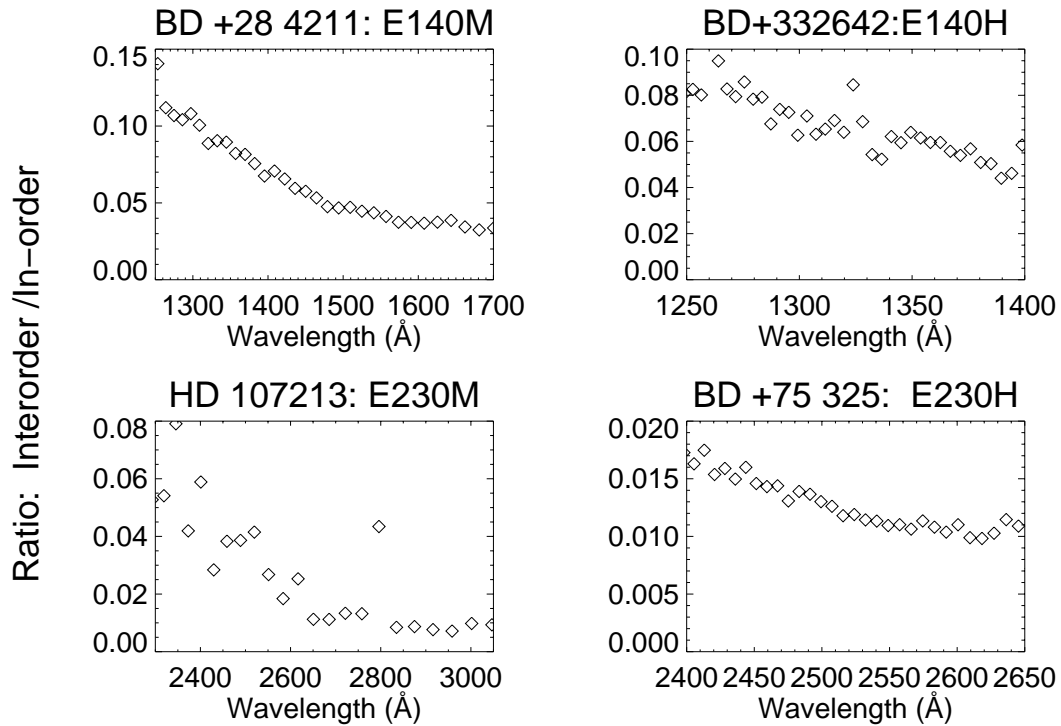


Figure 3. A deep pre-launch calibration E230H line lamp spectrum with a central wavelength of 2762 Å.

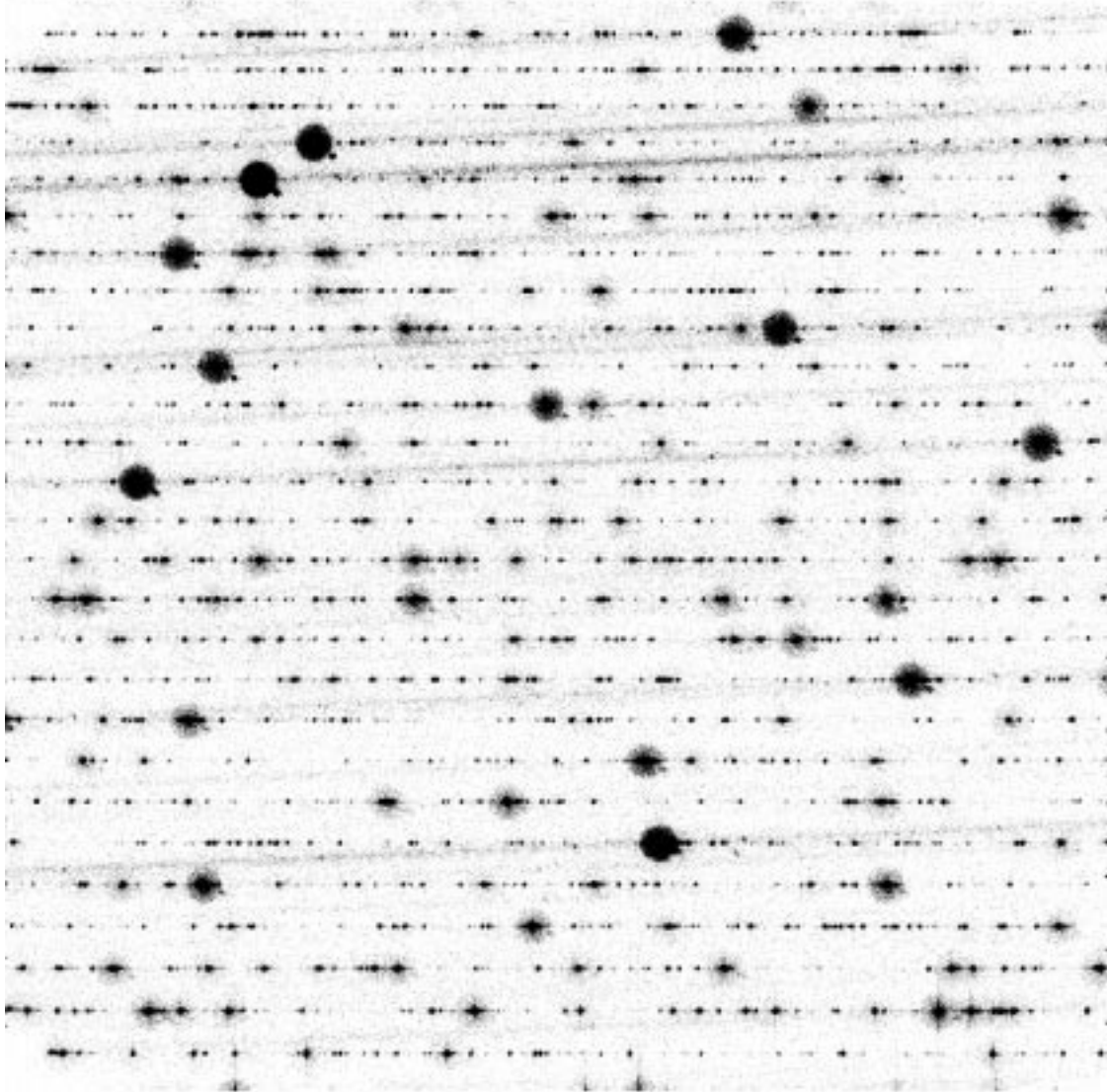


Figure 4. A post-launch E230H line lamp spectrum (O42704KGM) with a central wavelength of 2513 Å.

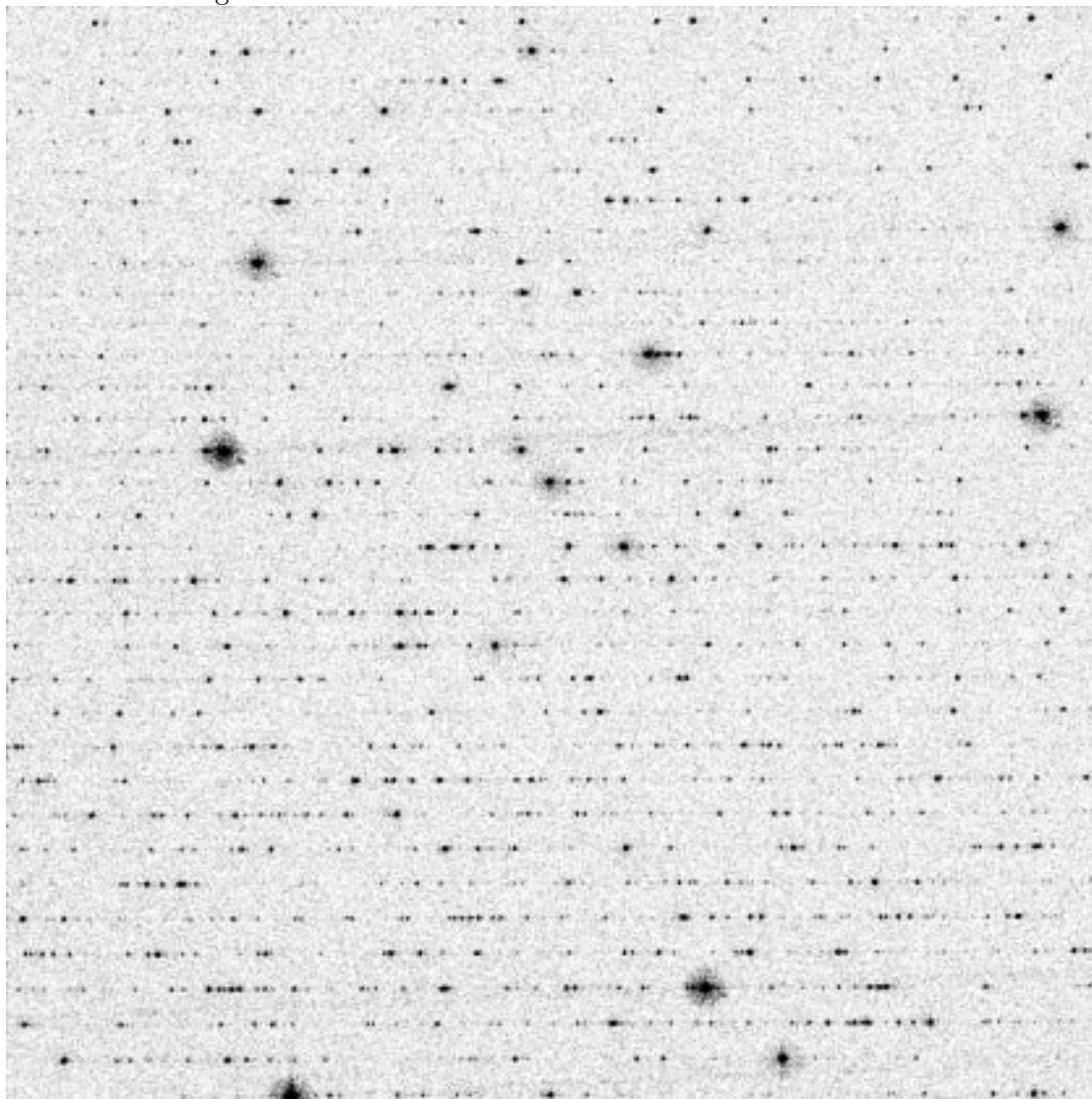
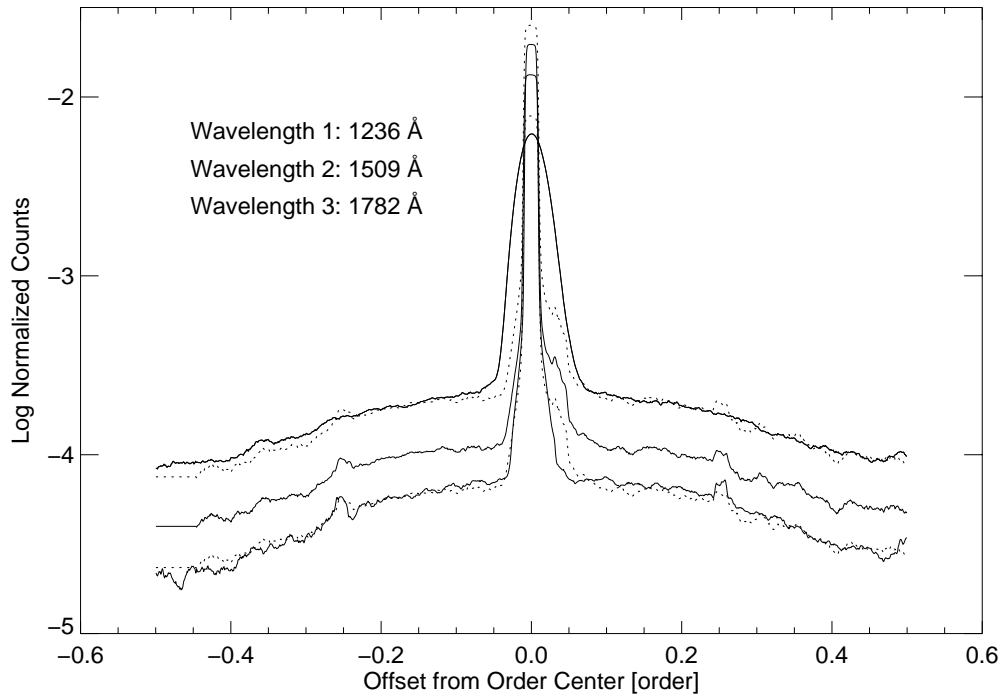


Figure 5. Laboratory measurement of the scattering profile of the E140M grating at three different wavelengths. The dotted lines show the predicted scattering profiles at 1230 Å and 1780 Å computed by scaling the 1509 Å scattering profile by  $\lambda^{-3.2}$ .



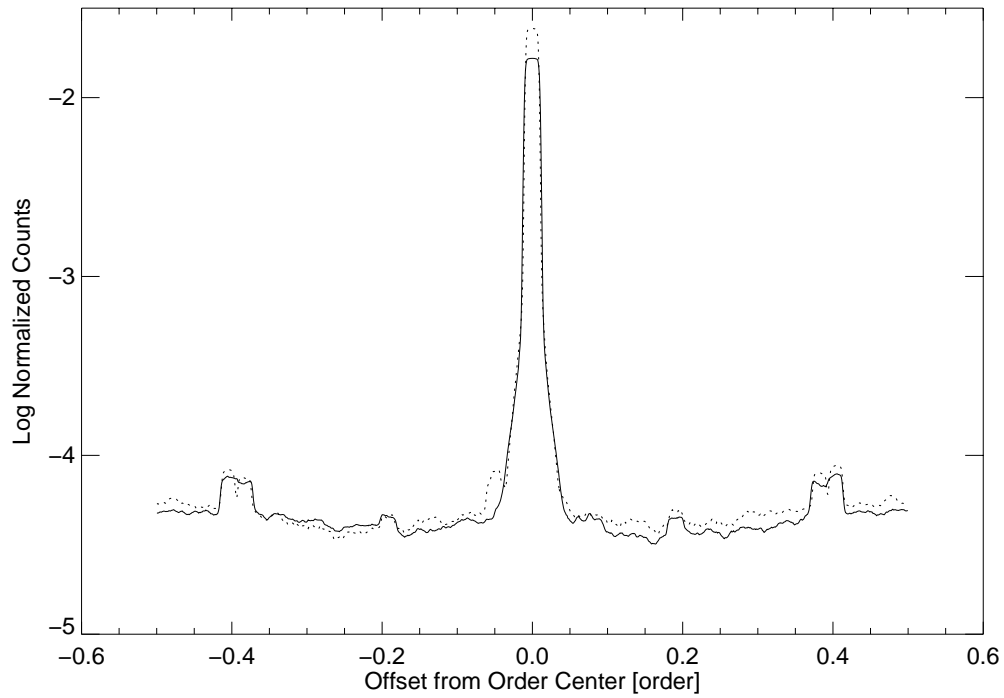
### 3. Laboratory Measurements of Echelle Scatter

The scattering properties of the STIS echelle gratings were studied prior to their integration into the instrument. Figure 5 shows the scattering function of the E140M grating at 1230 Å, 1509 Å, and 1780 Å. The amount of scattered light is found to be a strong function of wavelength, with a  $\lambda^{-3.2}$  dependence. On the other hand, the amount of scattering in the E140H grating shows little dependence on wavelength (Figure 6), at least for the two wavelengths measured. The scattering profile of the E140H grating is also flatter than that of the E140M grating, and shows more pronounced order ghosts.

### 4. Status

Unlike IUE or GHRS, the scattering in the STIS high-resolution modes appears to be dominated by scattering from the echelle grating, rather than from the cross-disperser. The non-local nature of echelle grating scatter makes a correction algorithm more difficult to implement. The most complete correction algorithm will likely be an iterative scheme, in which an initial spectrum is first extracted without any correction for scattered light, and then convolved with the echelle scattering function and detector response function. The amount of scattered light is then computed and used to correct the initial spectrum. A simpler local correction algorithm (e.g., Bianchi & Bohlin 1984) should still be useful where there are no strong variations in the continuum, or where the order overlap due to the detector halo is significant.

Figure 6. Laboratory measurement of the scattering profile of the E140H grating at 1509 Å (solid line) and 1782 Å (dotted line).



## References

- Bianchi, L., & Bohlin, R.C., 1984, *A&A*134, 31  
Cardelli, J.A., Ebbetts, D.C., & Savage, B.D., 1990, *ApJ*365, 789  
Heap, S., et al., 1997, *ApJ*, submitted  
Jenkins, E., et al., 1997, *ApJ*, submitted  
Walborn, N., et al., 1997, *ApJ*, submitted